



ISSN: 0067-2904

## Natural Radioactivity and its Hazards of Infracambrian Rocks at Jabal Sanam Structure, Southern Iraq

Safaa Al-Ali<sup>1</sup>, Sany Hannina<sup>1\*</sup>, Basim Soltan<sup>1</sup>, Khajak Vartanian<sup>2</sup>,  
Kareem Rukyees<sup>2</sup>

<sup>1</sup> Department of Geology, College of Science, University of Basrah, Basrah 61004, Iraq  
<sup>2</sup> Southern Directorate of Environment Protection, Radiation Department, Basrah 61001, Iraq

Received: 2/6/2022

Accepted: 10/8/2022

Published: 30/12/2022

### Abstract

The Jabal Sanam, a piercement salt plug, represents a unique geological phenomenon in southern Iraq. It is a remarkable geological landmark that rises about 141 m above sea level and covers approximately 2 km<sup>2</sup>, surrounded by flat areas on all sides. A radiological survey was conducted on the Jabal Sanam structure to determine the natural radioactivity levels and related radiation hazard indices. Eleven different rock types from several locations at Jabal Sanam were collected. An optical microscope and X-ray diffraction (XRD) were used to examine and identify the variable rock types in this structure. Natural radioactivity using field and laboratory equipment for these rocks was measured. The findings indicated that the average activity concentrations of the <sup>226</sup>Ra, <sup>232</sup>Th, and <sup>40</sup>K radionuclides of the Jabal Sanam rocks are 6.5 Bq kg<sup>-1</sup>, below the minimum detectable activity (MDA), and 83.3 Bq kg<sup>-1</sup>, respectively. The average radium equivalent (Raeq) activity value of the investigated rocks is 12.87 Bq kg<sup>-1</sup>, below the world recommended rate of 370 Bq kg<sup>-1</sup>. Moreover, the average absorbed dose rate (D<sub>γ</sub>) is 6.51 nGy h<sup>-1</sup> less than 60 nGy h<sup>-1</sup>. Furthermore, the average values of the external (H<sub>ex</sub>) and internal (H<sub>in</sub>) hazard indices are 0.035 and 0.052, respectively, which are also lower than the allowed limit value of 1.0 set by the international agencies. Overall, the findings of this investigation conclude that Jabal Sanam rocks do not have a radioactive health hazard.

**Keywords:** Natural radioactivity, radiation hazard, Infracambrian rocks, Jabal Sanam, Iraq.

تقييم مستويات النشاط الإشعاعي الطبيعي ومعايير المخاطر الإشعاعية لصخور تركيب جبل سنام ذات  
العمر الانفراكامبري، جنوب العراق

صفاء حسين العلي<sup>1</sup>، ساني إيليا حنين<sup>1\*</sup>، باسم حميد سلطان<sup>1</sup>، خاجاك وارتانان<sup>2</sup>، كريم رخيص<sup>2</sup>

<sup>1</sup> قسم علم الأرض، كلية العلوم، جامعة البصرة، البصرة، العراق

<sup>2</sup> قسم الإشعاع، دائرة حماية وتحسين البيئة، المنطقة الجنوبية، البصرة، العراق

\*Email: [sanyelia@yahoo.com](mailto:sanyelia@yahoo.com)

### الخلاصة

جبل سنام هو اسطوانة ملحية اختراقية تمثل ظاهرة جيولوجية فريدة في مدينة البصرة، جنوبي العراق. اذ يعد تركيب جيولوجي مميز يرتفع حوالي 141 متراً فوق مستوى سطح البحر ويغطي حوالي 2 كيلومتر مربع تحيط به مناطق مسطحة من جميع الجهات. اجريت عملية مسح اشعاعي للصخور هذا التركيب بهدف تقييم مستويات الاشعاع الطبيعي والصناعي. جمعت 11 عينة صخرية مختلفة من عدة مواقع في جبل سنام واستخدم المجهر البصري وتقنية حيود الأشعة السينية لفحص وتحديد أنواع الصخور المختلفة في هذا التركيب. تم قياس النشاط الإشعاعي الطبيعي لهذه الصخور باستخدام المعدات الميدانية والمختبرية. بينت النتائج أن معدل تركيز النشاط للنويدات المشعة في صخور جبل سنام هو 6.5 بكرل/كغم لـ  $^{226}\text{Ra}$  و اقل من الحد الأدنى للنشاط القابل للكشف لـ  $^{232}\text{Th}$  و 83.3 بكرل/كغم لـ  $^{40}\text{K}$ . معدل النشاط المكافئ للراديويم ( $\text{Ra}_{\text{eq}}$ ) لعينات صخور جبل سنام هو 12.87 بكرل/كغم وهو أقل من المعدل الموصى به عالمياً 370 بكرل/كغم. اما معدل الجرعة الممتصة فكان 6.51 نانو كراي/ساعة وهو اقل من المعدل المسموح به عالمياً 60 نانو كراي/ساعة. علاوة على ذلك، قيمة عامل المخاطر الخارجية ( $H_{\text{ex}}$ ) والمخاطر الداخلية ( $H_{\text{in}}$ ) كان 0.035 و 0.052 على التوالي وهي اقل كذلك من الحد المسموح به التي وضعتها الوكالات الدولية وحدة واحدة. بشكل عام، خلصت نتائج هذه الدراسة إلى أن صخور جبل سنام لا تشكل أي مخاطر اشعاعية على البيئة والصحة والسلامة.

### 1. Introduction

Natural radioactivity is everywhere on the Earth, even in some places that are more radioactive than others [1]. Humans are continuously interacting with the environment; accordingly, it is necessary to measure the radiation levels and potential radiological risks of  $\gamma$ -ray exposure to the human body and through inhalation of radioactive inert gases radon  $^{222}\text{Rn}$  and thoron  $^{220}\text{Rn}$  [2, 3]. The impact of radiation is mainly dependent on the content of the radionuclides in rocks, sediments, and soils. Long-lived radioactive isotopes include uranium  $^{238}\text{U}$  and  $^{235}\text{U}$  and thorium  $^{232}\text{Th}$ , and their decay products (daughters), in addition to potassium  $^{40}\text{K}$ , are the prime naturally-occurring radionuclides that make a significant contribution to the background activity (also called terrestrial background radiation) in most rocks [3–5].

However, radionuclides are widely occurring in nature; hence, the radiation level and doses vary from one place to another and primarily depend on the rock components [4]. The concentrations of uranium, thorium and potassium in common rocks are shown in Table 1. Uranium is most concentrated in sedimentary rocks, including coal, black shale and phosphates. Acidic igneous rocks are also enriched in uranium, but their concentration is relatively low compared to sedimentary rocks. Thorium predominantly occurs in acidic igneous rocks followed by bauxite deposits, shale and mudstone, while other rock types are below 7 ppm. Regarding potassium, it seems to be concentrated in most rocks as it occurs in quite common minerals, for example, feldspar mineral group, micas and some evaporite minerals such as sylvite (KCl) [5]. The high concentration of potassium in these rocks does not mean that all are radioactive, as only the least common  $^{40}\text{K}$  (0.01%) compares to the most common  $^{39}\text{K}$  (93.26%), and  $^{41}\text{K}$  (6.73%) is radioactive [6].

**Table 1:** Worldwide abundance of uranium, thorium and potassium in a wide range rocks [5, 7–18].

	Rock type	U (ppm)	Th (ppm)	K (wt%)
<b>Igneous rocks</b>	Syenite and phonolite	0.1-26	0.7-35	3-6
	Granite and rhyolite	2-50	8-56	2.5-4.5
	Intermediate rocks	1-6	8-56	2.5-4.5
	Mafic rocks	0.1-1	0.1-4	1-2
	Ultramafic	0.001-1	<0.1	~0.6
<b>Metamorphic rocks</b> <b>Sedimentary rocks</b>	Variable, typically	1-7	6-10	It depends on origin rocks
	Shale, clays mudstones	1-5	10-13	<0.01-7.1
	Black shales	2-1250	N/A	N/A
	Phosphorites	<700	1-5	N/A
	Sandstones	0.5-4	1-7	<0.01-5.6
	Limestone and dolomite	<0.1-9	0.05-3	0.3-0.6
	Coal, lignite and peat	1-6000	N/A	N/A
	Pure evaporite	<0.1	N/A	0
	Bauxite	N/A	~50	N/A
	Sylvite	N/A	N/A	52.4

N/A is not available.

Jabal Sanam is a unique geological phenomenon located in southern Iraq between (30°07'10"N – 30°08'00"N) and (47°37'10"E - 47°38'00"E). It rises about 96 m above the surrounding areas and covers approximately 2 km<sup>2</sup>. Numerous sedimentary, metamorphic and igneous Infracambrian rocks form this geological structure [19]. It also has several geological outcrops of the oldest rocks in Iraq, geological structures, valleys and caves, and several wild plants and animals. These features make it a destination site for researchers, school and university field trips, and local and international visitors. However, several initiatives to establish Jabal Sanam as a Geopark or Natural Park have been proposed in recent years [20]. Several challenges stood this idea, the most significant of which being the perception that the rocks were contaminated with radioactive elements due to military operations in this area during the Gulf Wars I and II. For establishing Jabal Sanam as a geopark or natural park, it is fundamental to measure the radioactivity levels of its rocks.

The previously published studies on radiation measurements at the Jabal Sanam and its surrounding areas are limited. Only two studies on one soil sample each were achieved by [21, 22], so this geological structure has not been studied in detail for radioactive level measurements for its forming rocks. Therefore, this article aims to measure the natural radioactivity levels and determine the radiation hazards associated with Infracambrian rocks that form the Jabal Sanam structure using field and laboratory equipment.

## 2. Geological setting

The Jabal Sanam is a piercement salt plug that represent a one of a kind geological structure located in southern Iraq. It is an interesting geological landmark surrounded by

flatlands on all sides (Figure 1), represented by the Dibdibba plain that was deposited during the Pleistocene [23]. The study area is characterized by a simple topographic surface and a slight elevation towards the northwest from the Iraqi lands and towards the east from the Arabian Gulf. The Jabal Sanam structure is situated within the Dibdibba plain according to [24], and within the quasi-platform foreland region according to the tectonic segmentation of Iraq [25].

It has complex semi-oval dome (Figure 1) that rises about 141 m above sea level. The trend of the long axis is NW-SE direction which extends approximately 1.7 km, while the short axis is about 1.5 km [20]. This dome is surrounded by several lateral folds and different types of normal and reverse faults, and numerous complex systems of joints and gypsum veins that are likely to be traced back in their inception to the influence of the intrusions process of salt rocks from deep levels towards the Earth's surface [26].



**Figure 1:** Location of the Jabal Sanam structure, southern Iraq.

It comprises interlocking rock beds in different directions in which various rock groups are intertwined (Figure 2). Thus, creating a representative and accurate stratigraphic column for the Jabal Sanam is challenging [19]. The Jabal Sanam rocks form what is known as complex cap rocks that represent the upper part of the salt dome. It consists mainly of evaporative rocks (gypsum) that represent the main body of the salt dome above the surface and constitute approximately 70% of its composition, known as a gypsum unit, topped by layers of finite thickness that are highly deformed and broken from clearly marly stacked limestone rocks [27]. These sequences are called the brecciated limestone unit. The lower part of the structure is composed of various sedimentary rocks, including dolomite rocks

alternated with red and green marl, gypsum rocks and compacted siltstone [19]. They may have been subjected to the regional metamorphic processes because they were at depths of about 10 km [27]. Before an eruption towards the Earth's surface, it formed a dolomite unit. The rocks of this unit have their original sedimentary sequence, despite being subjected to lifting and deformation processes during their intrusion to the surface. It is believed that the reason for this is that they were surrounded by flexible gypsum, which prevented them from the deformation processes. These rocks represent parts of the sedimentary rock sequences that were deposited during the Infracambrian period in this region, the so-called salts of the Hormuz Infracambrian series. Jabal Sanam also contains large pieces of igneous dolerite rocks that penetrated the salt rocks when they were in the shallow depths and were driven by rocks rushing with them towards the surface, in addition to various rocks such as chert, marble, schist, ironstones and others [28, 29].

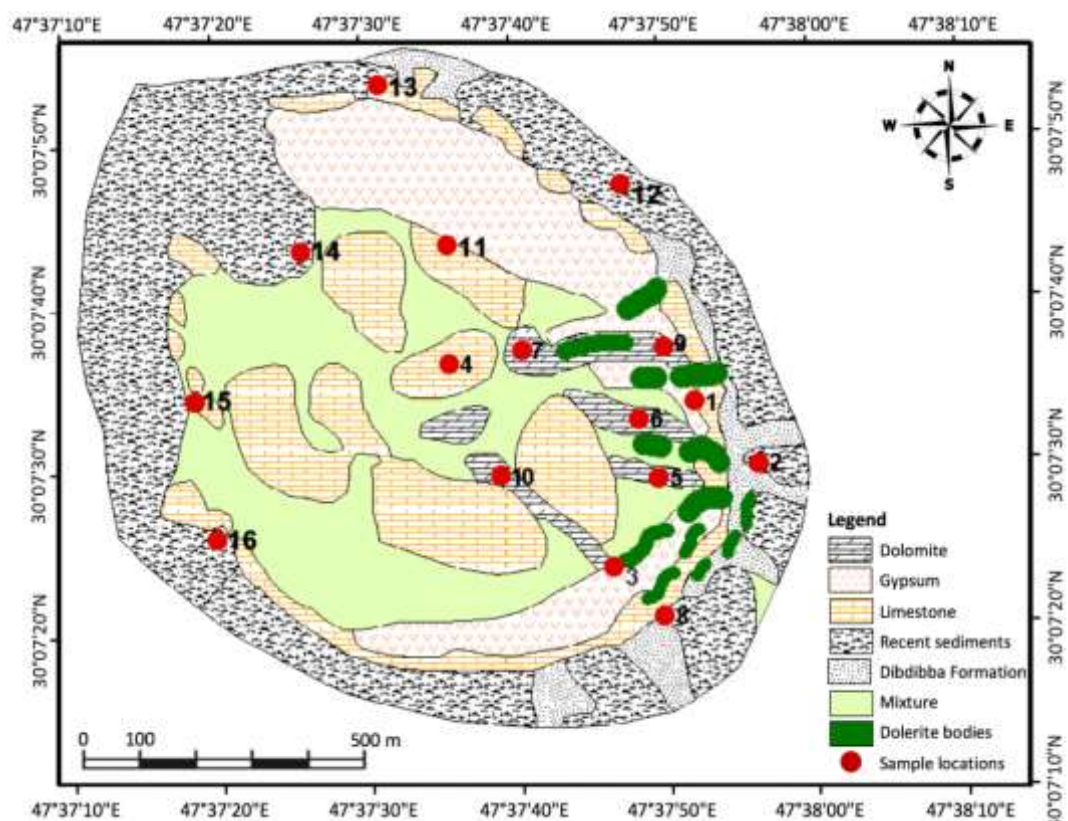


**Figure 2:** Geological map of Jabal Sanam and rock sample locations, modified after [19, 30].

The age of Jabal Sanam's rocks was estimated in the Infracambrian period (approximately 600 Ma), after determining the age of the igneous rocks by the dating method that was achieved by [24], which was found to be about 580 Ma. Furthermore, the age of the Jabal Sanam was concluded by comparison of the stratigraphic units of its rocks with the domes of the Infracambrian salts of Hormuz distributed in the southwestern region of Iran and the Arabian Gulf [31].

### 3. Materials and analytical methods

A detailed geological field survey was carried out on Jabal Sanam and its surrounding areas. Radiation measurements were taken to the rock beds and bodies (Plate 1). Overall, 11 rock samples of about 1 kg each from various locations throughout Jabal Sanam were collected (Figure 2). Petrographic studies were conducted using an optical polarised light microscope at the Department of Geology, University of Basrah, while XRD

measurements were carried out using Philips Type PW 1352 diffractometer at the Physics department, University of Basrah.

The samples were first measured in the field using GCA-07 and Gamma-Scout hand instruments equipped with Geiger-Muller tube to detect  $\gamma$ -ray and measure radiation dose rate (Plate 2A). The radiological measurements of the selected samples were repeated in the laboratory for verification and comparison using the same two devices. The field radiometers were calibrated using a standard  $^{137}\text{Cs}$ , and they can measure a dose rate on a wide scale of 0.01 up to 50.00  $\mu\text{Sv h}^{-1}$ . All samples were crushed into small particle sizes, homogenized, and dried at about 105 °C for 24 hours. Each sample weighing about 700 g and 1000 g was sealed into a standard Marinelli beaker, and the type of radioactive isotopes and their activity concentration were determined using the Gamma Counter Multichannel Analyser (type Kolga A 320) (Plate 2B). Energy calibration for the system was performed using radioactive standards of known energies  $^{137}\text{Cs}$  and  $^{60}\text{Co}$  calibration sources. The gamma-ray measurements were conducted at the Directorate of environment protection, Basrah, Iraq.



**Plate 1-** Field work, radiation measurements and collecting samples at Jabal Sanam: (A) The main gypsum unit outcrop in northern Jabal Sanam, (B) Field radiation measurements of limestone unit, (C) Beds of red marl, green marl, dolostone and gypsum of dolostone unit, (D)

Dolerite rock body, (E) Field radiation measurements of gypsum, (F) Field radiation measurements of Ironstones, (G) Chert sample and (H) Ironstone sample.

The activity concentration of  $^{226}\text{Ra}$  ( $^{238}\text{U}$ ) series was determined based on the  $\gamma$ -lines of its decay products including  $^{214}\text{Pb}$  at an energy of (295.22 KeV and 351.93 KeV) and  $^{214}\text{Bi}$  at an energy of (609.31 KeV, 1120.29 KeV, and 1764.49 KeV). The  $\gamma$ -lines of  $^{212}\text{Pb}$  at an energy of (238.63 KeV and 300.09 KeV),  $^{228}\text{Ac}$  at an energy of (338.40 KeV, 463.10 KeV, and 911.16 KeV), and  $^{208}\text{Tl}$  (583.19 KeV and 860.56 KeV) were used to estimate  $^{232}\text{Th}$  activity concentration. The activities of  $^{40}\text{K}$  and  $^{137}\text{Cs}$  were determined using the single  $\gamma$ -lines at energies of 1460.82 KeV and 661.66 KeV, respectively.

The minimum detectable activity (MDA) for each radionuclide was estimated to be 0.37 Bq  $\text{kg}^{-1}$  for  $^{214}\text{Pb}$ , 0.15 Bq  $\text{kg}^{-1}$  for  $^{214}\text{Bi}$ , 0.18 Bq  $\text{kg}^{-1}$  for  $^{212}\text{Pb}$ , 0.67 Bq  $\text{kg}^{-1}$  for  $^{228}\text{Ac}$ , 0.23 Bq  $\text{kg}^{-1}$  for  $^{208}\text{Tl}$ , 1.23 Bq  $\text{kg}^{-1}$  for  $^{40}\text{K}$ , and 0.09 Bq  $\text{kg}^{-1}$  for  $^{137}\text{Cs}$ .



**Plate 2-**(A) GCA-07 and Gamma-Scout hand instruments used for field radiation measurements, and (B) Gamma counter multichannel analyzer (type Kolga A 320) used for laboratory radiation measurements.

#### 4. Radiological hazard indices

The concentrations of  $^{226}\text{Ra}$ ,  $^{232}\text{Th}$  and  $^{40}\text{K}$  radionuclides are varied in soils and rocks; thus, different radiation indices to measure the  $\gamma$ -ray radiation risks associated with materials caused by these radionuclides were suggested. The radium equivalent activity ( $Ra_{eq}$ ) index is commonly utilized to determine the specific activity of rocks and soils that contain various radionuclide concentrations.  $Ra_{eq}$  is the total activities of  $^{226}\text{Ra}$ ,  $^{232}\text{Th}$  and  $^{40}\text{K}$  radionuclides, presuming that 370 Bq  $\text{kg}^{-1}$  of  $^{226}\text{Ra}$ , 259 Bq  $\text{kg}^{-1}$  of  $^{232}\text{Th}$  and 4810 Bq  $\text{kg}^{-1}$  of  $^{40}\text{K}$  generate the same dose rate of  $\gamma$ -ray [32]. This index is calculated using Eq. (1), which was first used by [32] and developed by [33, 34].

$$Ra_{eq}(\text{Bq kg}^{-1}) = 370 \left( \frac{C_{Ra}}{370} + \frac{C_{Th}}{259} + \frac{C_k}{4810} \right) = C_{Ra} + 1.43C_{Th} + 0.077C_k \quad (1)$$

Where  $C_{Ra}$ ,  $C_{Th}$  and  $C_k$  are the activity concentrations (in Bq  $\text{kg}^{-1}$ ) for  $^{226}\text{Ra}$ ,  $^{232}\text{Th}$  and  $^{40}\text{K}$ , respectively.

The absorbed dose rate ( $D\gamma$ ) can be used to determine the exposure to gamma radiation resulting from radioactive sources of  $^{226}\text{Ra}$ ,  $^{232}\text{Th}$  and  $^{40}\text{K}$  in the ground. It measures the absorbed rate of  $\gamma$ -ray dosage at 1 m above the level of the ground using Eq. (2). The absorbed dose rate conversion factor in the air from the actual contents of the above radionuclides was calculated by several researchers [35-38]. This work uses the factors for  $^{226}\text{Ra}$ ,  $^{232}\text{Th}$  and  $^{40}\text{K}$  were 0.4551, 0.5835 and 0.0429 nGy  $\text{h}^{-1}$  Bq  $\text{kg}^{-1}$ , respectively, as determined by [39].

Additionally, since the  $^{134}\text{Cs}$  and  $^{137}\text{Cs}$  are below the minimum detectable activity and ignored in this calculation.

$$D_{\gamma}(\text{nGy h}^{-1}) = 0.4551C_{Ra} + 0.5835C_{Th} + 0.0429C_K \quad (2)$$

Eq. 3 was employed to determine the annual effective dose rate (E). The conversion factor between the effective dose received by an adult and the absorbed dose in the air is considered  $0.7 \text{ Sv Gy}^{-1}$ . The factor of outdoor occupancy is 0.2 by assuming the average time people spend outdoors is 20% [3], and  $10^{-6}$  is the factor that converts nanometres to millimetres.

$$E_{\gamma}(\text{mSv y}^{-1}) = D_{\gamma} \times 8760 \times 0.2 \times 0.7 \times 10^{-6} \quad (3)$$

where  $D_{\gamma}$  is the absorbed dose rate in the air.

The external hazard index ( $H_{ex}$ ) is commonly utilized to calculate the external exposure of  $\gamma$ -ray emitted from the materials and then characterized its limiting value based on the acceptable equivalent dose, which must be less than unity [3, 40].  $H_{ex}$  can be calculated using Eq. 4 [32-34].

$$H_{ex} = \frac{C_{Ra}}{370} + \frac{C_{Th}}{259} + \frac{C_k}{4810} \quad (4)$$

Where  $C_{Ra}$ ,  $C_{Th}$  and  $C_k$  are the activity concentrations (in  $\text{Bq kg}^{-1}$ ) for  $^{226}\text{Ra}$ ,  $^{232}\text{Th}$  and  $^{40}\text{K}$ , respectively.

The internal hazard index ( $H_{in}$ ) is also necessary to be calculated which indicates the exposure to inert radon gas ( $^{222}\text{Rn}$ ) and its short-lived secondary daughters [34, 41].  $H_{in}$  was computed using Eq. 5 suggested by [34]:

$$H_{in} = \frac{C_{Ra}}{185} + \frac{C_{Th}}{259} + \frac{C_k}{4810} \quad (5)$$

Where  $C_{Ra}$ ,  $C_{Th}$  and  $C_k$  are the activity concentrations (in  $\text{Bq kg}^{-1}$ ) for  $^{226}\text{Ra}$ ,  $^{232}\text{Th}$  and  $^{40}\text{K}$ , respectively.

## 5. Results and discussion

### 5.1 Mineralogy and petrography

The collected rock samples from Jabal Sanam representing this geological structure's most common rock types were studied. The polarized light microscope was used to examine the thin sections of these rocks as shown in (Plate 3), and some of them were examined using XRD technique illustrated in (Figure 3) to determine their rock-forming minerals and the identity of each rock type to be linked with the radiation measurements of each one. Green and red marl rocks are diagnosed by being composed of fine-grained clay minerals that are difficult to be identified under the ordinary polarized microscope and thus were roughly diagnosed through XRD.

Dolostone is composed of clear rhombic dolomite crystals with pronounced binary cleavage (Plate 3A), and the XRD showed that dolomite is the predominant mineral in addition to a minor amount of quartz and gypsum (Figure 3A). Limestone seems exposed to a highly solidification process and is characterized by the microcrystalline (micritic) texture of calcite minerals and the absence of fossils (Plate 3B).

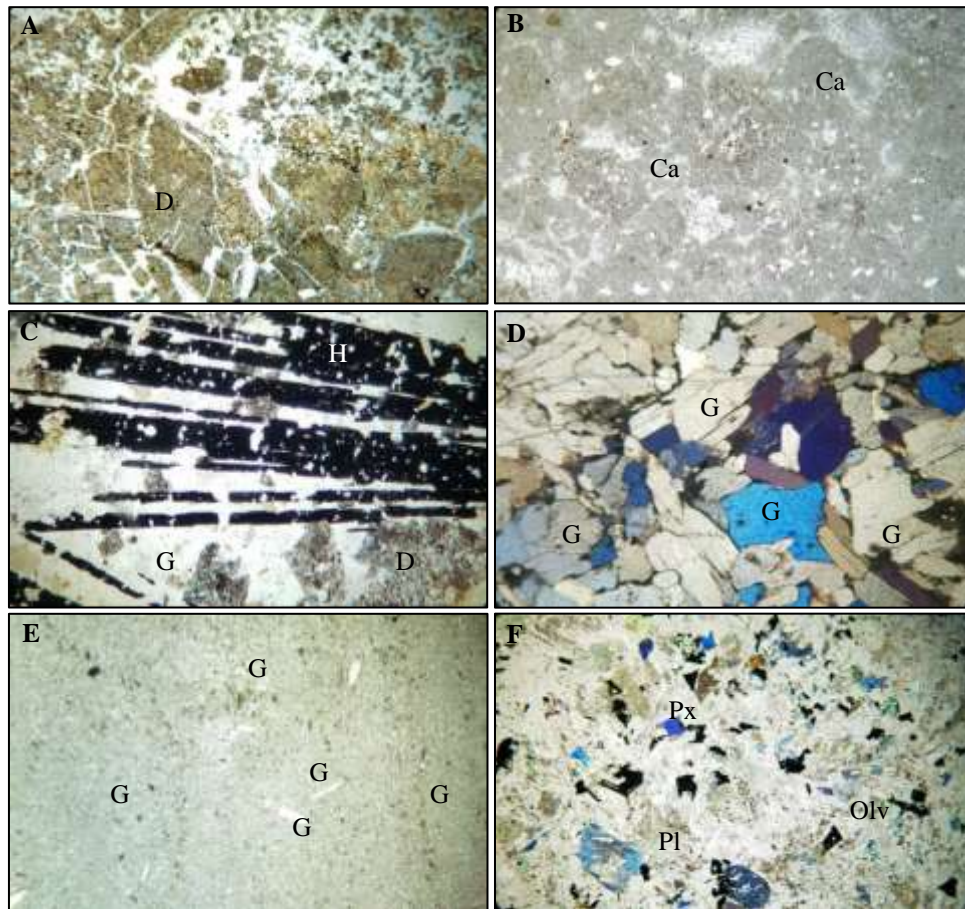


**Plate 3-** Rock thin sections of selected samples: (A) dolomite rhombic crystals in dolomite rock, (B) micritic limestone, (C) hematite opaque lathes in ironstone, (D) coarse-grained gypsum, (E) fine-grained gypsum, and (F) plagioclase and pyroxene minerals in dolerite igneous rock. Magnification x 40, XPL. Abbreviations: Ca: calcite, D: dolomite, G: gypsum, H: hematite, Pl: plagioclase, Px: pyroxene, and Olv: olivine.

Sedimentary ironstones contain a high amount of iron oxide minerals and sometimes large opaque crystals of hematite mineral together with calcite and gypsum, as shown in Plate 3C and indicated by the XRD in Figure 3C. The gypsum rock represents the most common rock type at Jabal Sanam. In the field, gypsum crystals range from large crystal size in crystallized gypsum (Plate 3D) to fine crystal size in microcrystalline gypsum (Plate 3E). Under the microscope, they characterized by large crystal sizes and sometimes called microcrystalline or alabastrine texture as well as the porphyritic texture, which reflects various crystallization conditions of gypsum [27]. The gypsum is the predominant mineral, in addition to a minor amount of quartz and dolomite (Figure 3D). Chert rocks appeared under the microscope consisting of microcrystalline quartz and sometimes polycrystalline, with the absence of any traces of fossils, which indicates their chemical origin in their formation [31] with a clear content of iron oxides, which gave these rocks a distinguished dark brown colour in hand samples.

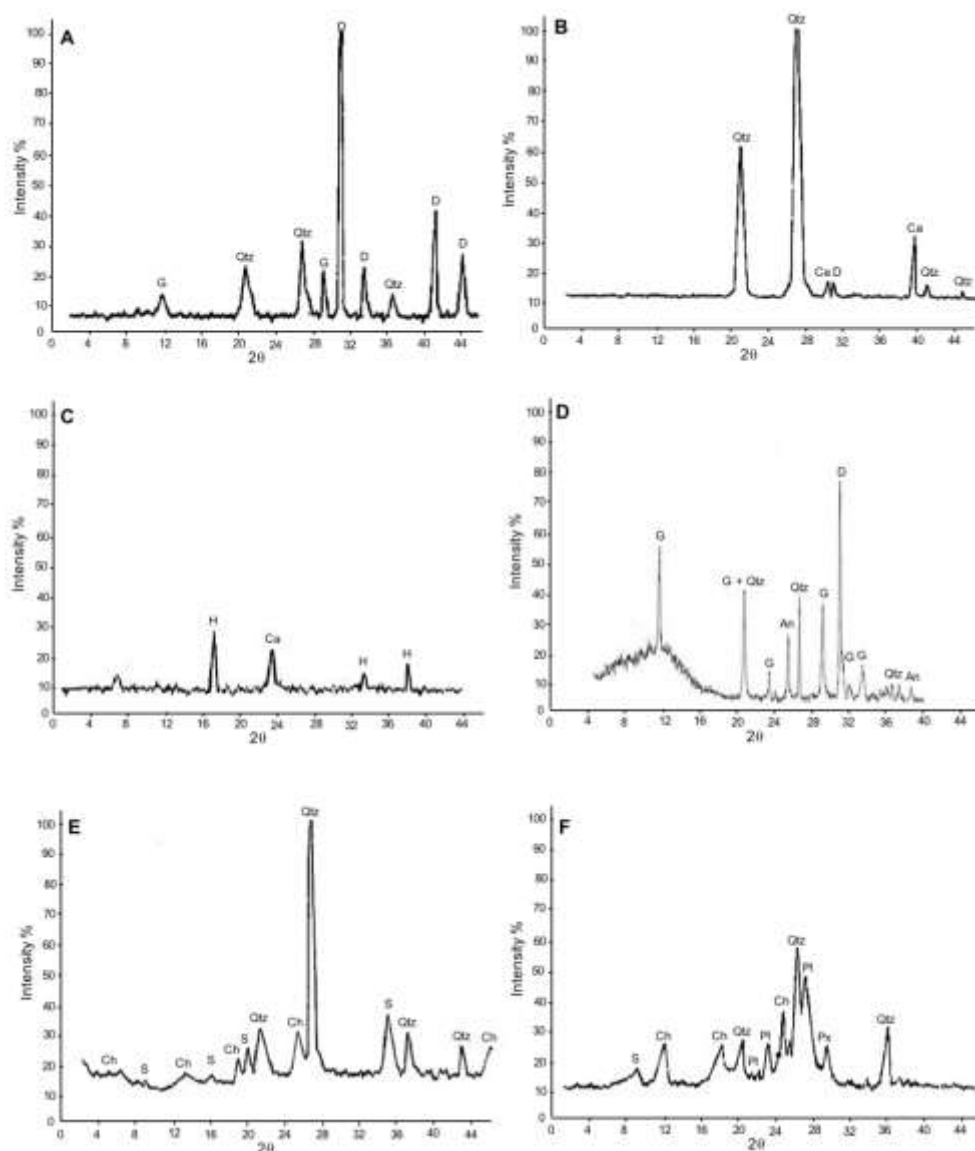


**Figure 3:** XRD profile of the studied rock samples (A) Dolostone (B) Limestone (C) Ironstone (D) Gypsum (E) Chert and (F) Dolerite. Abbreviations: An: anhydrite, Ca: calcite, Ch: chlorite, D: dolomite, G: gypsum, H: hematite, Pl: plagioclase, Px: pyroxene, Qtz: quartz and S: sericite.

The main igneous rock at the Jabal Sanam is dolerite. This rock consists of plagioclase feldspar minerals (Plate 3F) with distinctive elongate lath shapes formed with other minerals such as pyroxene, olivine and iron oxides, various delicate textures such as ophitic and subophitic textures were recognized.

## 5.2 Radiological measurements

### a. Activity concentration

The specific activities of  $^{226}\text{Ra}$ ,  $^{232}\text{Th}$ ,  $^{40}\text{K}$ ,  $^{134}\text{Cs}$ , and  $^{137}\text{Cs}$  in the studied samples in the Jabal Sanam area are listed in Table 2. As indicated from these data, the highest activity concentration in the collected samples originates from  $^{40}\text{K}$ , which ranges between  $34.4 \pm 1.6$  Bq  $\text{kg}^{-1}$  in chert and  $132.0 \pm 2.7$  Bq  $\text{kg}^{-1}$  in ironstone with an average activity of  $83.3$  Bq  $\text{kg}^{-1}$ .

The remaining activity concentration originates from  $^{226}\text{Ra}$ , which ranges between  $4.6\pm 1.0$  Bq  $\text{kg}^{-1}$  in shale and  $8.3\pm 2.0$  Bq  $\text{kg}^{-1}$  in green marl, while  $^{232}\text{Th}$  is lower than the minimum detectable activity in all rock samples. It is worth noting that  $^{134}\text{Cs}$  and  $^{137}\text{Cs}$  were also less than the minimum detectable activity in all samples.

Although the activity concentration of  $^{226}\text{Ra}$ ,  $^{232}\text{Th}$  and  $^{40}\text{K}$  in the analyzed rock samples are below their average worldwide activity concentration of 32, 45, and 420 Bq  $\text{kg}^{-1}$ , respectively [3], their levels vary from one sample to another depending on the rock type, mineralogical composition, and radionuclide content in each rock. For example, as was pointed out in Section 2 and confirmed by the fieldwork, the most common rock type at Jabal Sanam is gypsum which forms approximately 70% of its components [27] with a thickness of about 70 m. Consequently, this evaporative rock represents the core and most of the exterior part of the Jabal Sanam structure, which has almost null activity concentration according to the radiation measurements.

**Table 2:** The measured activity concentration of natural and anthropogenic radionuclides in the rocks of Jabal Sanam, southern Iraq.

Sample number	Weight (kg)	Lithology	Activity concentration (Bq $\text{kg}^{-1}$ )				
			$^{226}\text{Ra}$	$^{232}\text{Th}$	$^{40}\text{K}$	$^{134}\text{Cs}$	$^{137}\text{Cs}$
JS1	0.80	Marly limestone	$7.1\pm 2.0$	<MDA	$41.8\pm 1.6$	<MDA	<MDA
JS2	0.70	Limestone	$7.2\pm 2.0$	<MDA	$88.5\pm 2.6$	<MDA	<MDA
JS3	0.70	Dolerite	$6.8\pm 1.0$	<MDA	$121.0\pm 3.1$	<MDA	<MDA
JS4	0.75	Limestone	$5.3\pm 1.0$	<MDA	$79.8\pm 1.6$	<MDA	<MDA
JS5	0.80	Shale	$4.6\pm 1.0$	<MDA	$79.3\pm 2.3$	<MDA	<MDA
JS6	0.90	Dolostone	$8.2\pm 2.0$	<MDA	$129.0\pm 2.7$	<MDA	<MDA
JS7	0.75	Red marl	$5.1\pm 1.0$	<MDA	$69.7\pm 2.3$	<MDA	<MDA
JS8	1.00	Ironstone	$5.9\pm 1.0$	<MDA	$132.0\pm 2.7$	<MDA	<MDA
JS9	0.95	Green marl	$8.3\pm 2.0$	<MDA	$93.5\pm 2.3$	<MDA	<MDA
JS10	0.70	Chert	$6.4\pm 1.0$	<MDA	$34.4\pm 1.6$	<MDA	<MDA
JS11	0.95	Gypsum	$6.1\pm 1.0$	<MDA	$47.6\pm 1.6$	<MDA	<MDA
Min			4.6	<MDA	34.4	<MDA	<MDA
Max			8.3	<MDA	132.0	<MDA	<MDA
Average			6.5	<MDA	83.3	<MDA	<MDA

Note: MDA is minimum detectable activity. The activity concentration of  $^{226}\text{Ra}$  ( $^{238}\text{U}$ ) series was determined based on the  $\gamma$ -lines of  $^{214}\text{Pb}$  and  $^{214}\text{Bi}$ ,  $^{232}\text{Th}$  from  $\gamma$ -lines of  $^{212}\text{Pb}$ ,  $^{228}\text{Ac}$  and  $^{208}\text{Tl}$ , and  $^{40}\text{K}$ ,  $^{134}\text{Cs}$  and  $^{137}\text{Cs}$  directly from their  $\gamma$ -lines.

The finding indicates that the total activity concentration of  $^{226}\text{Ra}$ ,  $^{232}\text{Th}$  and  $^{40}\text{K}$  radionuclides is less than the world recommended limit of 370 Bq  $\text{kg}^{-1}$  [3]. Furthermore, the activity concentration of anthropogenic radionuclides  $^{134}\text{Cs}$  and  $^{137}\text{Cs}$  are below the detection limit and so have no contribution to the overall radiation exposure. Moreover, the activity concentration of  $^{226}\text{Ra}$  in this investigation is consistent with the previously published finding by [21], Table 3.

There were no available data  $^{232}\text{Th}$ , while the average activity of  $^{40}\text{K}$  in this investigation is moderately less than the measured value by [22]. The latter took a soil sample from an area about 2 km north of the Jabal Sanam. Thus, a high amount of  $^{40}\text{K}$  could be caused by the existence of potassium-rich clay minerals, for example, illite and illite-montmorillonite mixed layers in this area. These clay minerals are common in Basrah's sediments and soils [42, 43]. The sediment in this area could be mainly influenced by the presence of K-feldspar, widespread in this area [44].

**Table 3:** The average radionuclide activity concentration of this study compared with previously published measurements

Sample type	Activity concentration (Bq kg <sup>-1</sup> )					Reference
	<sup>226</sup> Ra	<sup>232</sup> Th	<sup>40</sup> K	<sup>137</sup> Cs	<sup>134</sup> Cs	
Rocks	6.46	<MDA	83.33	<MDA	<MDA	This study
Soil	3.7	N/A	N/A	N/A	N/A	[21]
Soil	N/A	N/A	1310.9	N/A	N/A	[22]

Note: N/A is not available and MDA is minimum detectable activity.

#### b. Radiological hazard indices

The results of these calculated indices for the collected rocks of Jabal Sanam area are presented in Table 4.

It is apparent from this table that all radiological hazard indices are slightly different from one sample to another. The highest index values are in dolostone, and the lowest are in chert. The radium equivalent activity ( $R_{\text{eq}}$ ) values for all investigated rocks range from 9.05 Bq kg<sup>-1</sup> to 18.13 Bq kg<sup>-1</sup> and have an average value of 12.87 Bq kg<sup>-1</sup>. These indices are below the permitted limit of 370 Bq kg<sup>-1</sup> [3].

The absorbed dose rate ( $D\gamma$ ) ranges between 4.39 nGy h<sup>-1</sup> and 9.27 nGy h<sup>-1</sup> with an average rate of 6.51 nGy h<sup>-1</sup>, which is below the rate of 60 nGy h<sup>-1</sup> established by [3]. Regarding the annual effective dose rate ( $E\gamma$ ), its rates range between 0.005 mSv y<sup>-1</sup> and 0.011 mSv y<sup>-1</sup> and have an average dose rate of 0.008 mSv y<sup>-1</sup>. These rates are not exceeded the worldwide outdoor upper level of 0.07 mSv y<sup>-1</sup> [3]. Consequently, it is an acceptable value and causes no radiation hazards.

**Table 4:** The calculated radium equivalent activity ( $Ra_{eq}$ ), absorbed dose rate ( $D_\gamma$ ), annual effective dose rate ( $E_\gamma$ ), external and internal hazard indices ( $H_{ex}$  and  $H_{in}$ ), along with annual measured dose rate in the rocks collected from Jabal Sanam, southern Iraq.

Sample number	Lithology	Radiological hazard indices					Measured dose rate * mSv y <sup>-1</sup>
		$Ra_{eq}$ Bq kg <sup>-1</sup>	$D_\gamma$ nGy h <sup>-1</sup>	$E_\gamma$ mSv y <sup>-1</sup>	$H_{ex}$	$H_{in}$	
JS1	Marly limestone	10.32	5.02	0.006	0.03	0.05	1.31
JS2	Limestone	14.01	7.07	0.009	0.04	0.06	1.31
JS3	Dolerite	16.12	8.29	0.010	0.04	0.06	0.96
JS4	Limestone	11.44	5.84	0.007	0.03	0.05	1.31
JS5	Shale	10.71	5.50	0.007	0.03	0.04	1.14
JS6	Dolostone	18.13	9.27	0.011	0.05	0.07	1.31
JS7	Red marl	10.47	5.31	0.007	0.03	0.04	1.05
JS8	Ironstone	16.06	8.35	0.010	0.04	0.06	1.40
JS9	Green marl	15.50	7.79	0.010	0.04	0.06	1.40
JS10	Chert	9.05	4.39	0.005	0.02	0.04	1.31
JS11	Gypsum	9.77	4.82	0.006	0.03	0.04	0.88
Min		9.05	4.39	0.005	0.02	0.04	0.88
Max		18.13	9.27	0.011	0.05	0.07	1.40
Average		12.87	6.51	0.008	0.03	0.05	1.22

\* Direct measurement using hand equipment (average of three readings).

The external hazard index ( $H_{ex}$ ) ranges between 0.024 and 0.049 with an average value of 0.035, which is much lower than the safe limit of 1.0 [3]. The internal hazard index ( $H_{in}$ ) ranges between 0.041 and 0.071, with an average of 0.052. This value is also below the limit value of 1.0, implying that all rock samples are not sources of internal hazard caused by radon and its short-lived daughters.

Furthermore, the direct measurements carried out in the field using Gamma-Scout equipment showed the annual dose rate from all rock types range between 0.88 mSv y<sup>-1</sup> and 1.40 mSv y<sup>-1</sup> and an average rate of 1.22 mSv y<sup>-1</sup>. It is worth mentioning that the annual dose rate of this study is close to the previously reported rate of 1.14 mSv y<sup>-1</sup> by [21]. According to the EU legal upper limits, these averages are lower than the allowable dosage rate of 20 mSv y<sup>-1</sup> and 6 mSv y<sup>-1</sup> for categories A and B, respectively, presuming 2000 working hours per year [45].

It can thus be inferred from the above radiological indices that all rock samples at Jabal Sanam are below the worldwide limits and would not present significant external and internal radiation hazards that could affect human health.

## 6. Conclusions

The main objectives were to measure and assess the natural radioactivity levels and related radiation hazard indices of various rock types collected from the Jabal Sanam structure. According to activity concentration and radiological hazard indices, it can be concluded that all rock types at the Jabal Sanam showed very low activity of <sup>226</sup>Ra, <sup>232</sup>Th, and <sup>40</sup>K radionuclides below the worldwide allowed limit since gypsum forms the widespread and thickest rock type of this structure with almost null radiation level. The radiological hazard

indices of these rocks are below the recommended limits. Accordingly, the Jabal Sanam rocks do not have a radioactive health hazard so they can be established as a potential geopark or natural park in the future.

## 7. Acknowledgements

The authors did not receive any specific grant from the public, commercial, or not-for-profit funding agencies for conducting this study. The authors would like to acknowledge the Department of Physics at the College of Science, University of Basrah, for using a field radiometer.

## References

- [1] D. Holmes, "Radioactivity in the environment: The hazards and benefits the hazard," 2004.
- [2] S. S. Johnson, "Natural radiation," *Virginia Minerals*, vol. 37, pp. 9–16, 1991.
- [3] UNSCEAR, "Sources and effects of ionizing radiation," United Nations Scientific Committee on the Effect of Atomic Radiation, United Nations, New York, 2000.
- [4] M. Tzortzis and H. Tsertos, "Determination of thorium, uranium and potassium elemental concentrations in surface soils in Cyprus," *Journal of Environmental Radioactivity*, vol. 77, pp. 325–338, 2004, [Online]. Available: <https://doi.org/10.1016/j.jenvrad.2004.03.014>.
- [5] A. M. Tye, A. E. Milodowski, and P. L. Smedley, "Distribution of natural radioactivity in the environment," 2017.
- [6] K. J. R. Rosman and P. D. P. Taylor, "Isotopic compositions of the elements 1997 (Technical Report)," *Pure and Applied Chemistry*, vol. 70, pp. 217–235, 1998, [Online]. Available: <https://doi.org/10.1351/pac199870010217>.
- [7] K. H. Wedepohl, *Handbook of Geochemistry: Volume II/5 Elements La (57) to U (92)*. Springer-Verlag, Berlin Heidelberg and New York, 1978.
- [8] S. H. Bowie, "The mode of occurrence and distribution of uranium deposits. Philosophical Transactions of the Royal Society of London. Series A, , 291:289-300," *Mathematical and Physical Sciences*, 1979, [Online]. Available: <https://doi.org/10.1098/rsta.1979.0027>.
- [9] T. K. Ball and A. E. Milodowski, "The geological, geochemical, topographical and hydrogeological characteristics of the Broubster natural analogue site, Caithness," 1989.
- [10] D. K. Hobday and W. E. Galloway, "Groundwater processes and sedimentary uranium deposits," *Hydrogeology Journal*, vol. 7, pp. 127–138, 1999, [Online]. Available: <https://doi.org/10.1007/s100400050184>.
- [11] R. M. Hazen, R. C. Ewing, and D. A. Sverjensky, "Evolution of uranium and thorium minerals," *American Mineralogist*, vol. 94, pp. 1293–1311, 2009, [Online]. Available: <https://doi.org/10.2138/am.2009.3208>.
- [12] R. J. Howell, J. Grogan, M. Hutton-Ashkenny, C. Brough, K. Penman, and D. J. Sapsford, "Geometallurgy of uranium deposits," *Minerals Engineering*, vol. 24, pp. 1305–1313, 2011, [Online]. Available: <https://doi.org/10.1016/j.mineng.2011.05.005>.
- [13] M. Cuney, "Evolution of uranium fractionation processes through time: driving the secular variation of uranium deposit types," *Economic Geology*, vol. 105, pp. 553–569, 2010.
- [14] O. P. Kreuzer, V. Markwitz, A. K. Porwal, and T. C. McCuaig, "A continent-wide study of Australia's uranium potential: Part I: GIS-assisted manual prospectivity analysis," *Ore Geology Reviews*, vol. 38, pp. 334–366, 2010, [Online]. Available: <https://doi.org/10.1016/j.oregeorev.2010.08.003>.
- [15] G. B. Douglas, C. R. Butt, and D. J. Gray, "Geology, geochemistry and mineralogy of the lignite-hosted Ambassador palaeochannel uranium and multi-element deposit, Gunbarrel Basin, Western Australia," *Mineralium Deposita*, vol. 46, pp. 761–787, 2011, [Online]. Available:

- <https://doi.org/10.1007/s00126-011-0349-4>.
- [16] M. Fayek, J. Horita, and E. M. Ripley, "The oxygen isotopic composition of uranium minerals: A review," *Ore Geology Reviews*, vol. 41, pp. 1–21, 2011, [Online]. Available: <https://doi.org/10.1016/j.oregeorev.2011.06.005>.
- [17] S. A. Cumberland, G. Douglas, K. Grice, and J. W. Moreau, "Uranium mobility in organic matter-rich sediments: A review of geological and geochemical processes," *Earth-Science Reviews*, vol. 159, pp. 160–185, 2016, [Online]. Available: <https://doi.org/10.1016/j.earscirev.2016.05.010>.
- [18] J. Guidez and S. Gabriel, "Extraction of uranium from seawater: a few facts," *EPJ Nuclear Sciences and Technologies*, vol. 2, p. 10, 2016, [Online]. Available: <https://doi.org/10.1051/epjn/e2016-50059-2>.
- [19] B. H. Soltan, "Petrology and origin of Jabal Sanam structure, southern Iraq," Unpublished dissertation, University of Basrah, (in Arabic with English abstract), 2002.
- [20] B. H. Soltan, "Characteristic Features of the Proposed Jabal Sanam Geopark- Southern Iraq," *Geoheritage*, vol. 13, pp. 1–13, 2021, [Online]. Available: <https://doi.org/10.1007/s12371-021-00599-z>.
- [21] S. M. Potrous and K. F. Wartan, "Surface structures studies for samples contaminated with depleted uranium," *Basrah Researches Sciences Journal*, vol. 32, pp. 1–11, 2006.
- [22] A. J. Bashar, A. A. Al Muhyi, M. K. Al-Tememi, and N. K. Alalwan, "Determination of the Specific Activity for the natural radioactive isotopes (<sup>40</sup>K, <sup>212</sup>Pb, <sup>214</sup>Pb, <sup>214</sup>Bi, <sup>228</sup>Ac) in soils and sediments for selected areas of the marshes southern Iraq, Basra province and the northern Arabian Gulf," *Marsh Bulletin*, vol. 11, pp. 102–111, 2016.
- [23] T. Buday, "The regional geology of Iraq: stratigraphy and paleogeography," vol. 1. State Organization for Minerals, Directorate General for Geological Survey and Mineral Investigations, 1980.
- [24] T. Buday and S. Z. Jassim, "The Regional Geology of Iraq," vol. 2: Tectonism, Magmatism and Metamorphism. Iraq Geological Survey Publications, Baghdad, Iraq, 1987.
- [25] N. M. S. Numan, "Discussion on: Dextral Transpression in Late Cretaceous Continental collision, Sanandaj-Sirjan Zone, Western Iran," *Journal of Structural Geology*, vol. 23, pp. 2033–2034, 2001.
- [26] W. G. Al-Muttory, "Structure and tectonism of Jabal Sanam southern Iraq," Unpublished dissertation, University of Basrah (in Arabic with English abstract), 2002.
- [27] A. M. Al-Hamdani, A. H. Al-Marsoumi, and B. H. Soltan, "Petrography and mineralogy of Jabal Sanam gypsum rocks, southern Iraq," *Iraqi National Journal of Earth Sciences*, vol. 5, pp. 18–29, 2005.
- [28] K. M. Al-Naqib, "Geology of Jabal Sanam, South Iraq," *Journal of the Geological Society of Iraq*, vol. 3, no. 9–36, 1970.
- [29] K. S. Al-Bassam, "Petrology and chemistry of some exotic rock fragments from Jabal Sanam, Basrah, Iraq," *Iraqi Bulletin of Geology and Mining*, vol. 7, pp. 39–53, 2011.
- [30] A. K. Al-Ali, "Hypsometric analysis of Jabal Sanam–southern Iraq–using GIS," *Journal of Basrah Researches (Sciences)*, vol. 41, pp. 15-25, 2015.
- [31] B. H. Soltan, "Petrology and stratigraphy of pre-Cambrian Hormuz Series outcrops in Jabal Sanam structure-the oldest surface rocks in Iraq," *Basrah Journal of Science*, vol. 38, pp. 497–520, 2020.
- [32] E. M. Krisiuk, S. I. Tarasov, V. P. Shamov, N. I. Shalak, E. P. Lisachenko, and L. G. Gomelsky, "A study on radioactivity in building materials," 1971.
- [33] E. Stranden, "Some aspects on radioactivity of building materials," *Physica Norvegica*, vol. 8, pp. 163–167, 1976.

- [34] R. Krieger, "Radioactivity of construction materials," *Betonwerk Fertigteil Techn*, vol. 47, pp. 468–473, 1981.
- [35] H. L. Beck, "Exposure rate conversion factors for radionuclides deposited on the ground," 1980.
- [36] K. Saito and P. Jacob, "Gamma ray fields in the air due to sources in the ground," *Radiation Protection Dosimetry*, vol. 58, pp. 29–45, 1995, [Online]. Available: <https://doi.org/10.1093/oxfordjournals.rpd.a082594>.
- [37] K. K. Ali, "Radioactivity in building materials in Iraq," *Radiation Protection Dosimetry*, vol. 148, no. 3, pp. 372–379, 2012.
- [38] K. K. Ali, "Radionuclides content and the radiological hazard of sediment of the Euphrates River and sprigs-western Iraq," *Iraqi Journal of Science*, vol. 56, no. 2A, pp. 1098–1110, 2015.
- [39] L. S. Quindos, P. L. Fernandez, C. Rodenas, J. Gomez-Arozamena, and J. Arteché, "Conversion factors for external gamma dose derived from natural radionuclides in soils," *Journal of Environmental Radioactivity*, vol. 71, pp. 139–145, 2004, [Online]. Available: [https://doi.org/10.1016/S0265-931X\(03\)00164-4](https://doi.org/10.1016/S0265-931X(03)00164-4).
- [40] NEA, "Exposure to radiation from the natural radioactivity in building materials," Nuclear Energy Agency, 1979.
- [41] J. Beretka and P. J. Matthew, "Natural radioactivity of Australian building materials, industrial wastes and by-products," *Health Physics*, vol. 48, pp. 87–95, 1985, [Online]. Available: <https://doi.org/10.1097/00004032-198501000-00007>.
- [42] S. N. Al-Mussawy and M. A. Basi, "Clay minerals of suspended matter and surficial sediments of Khor Al-Zubair estuary, NW Arabian Gulf," *Estuarine, Coastal and Shelf Science*, vol. 36, pp. 183–193, 1993, [Online]. Available: <https://doi.org/10.1006/ecss.1993.1012>.
- [43] S. H. Al-Ali, "Geochemical and mineralogical study of the fluvial deposits at Abul Khasib area, south east of Iraq," *Mesopotamia Journal of Marine Science*, vol. 25, pp. 154–165, 2010.
- [44] S. J. Al-Khafaji, S. H. Al-Ali, and H. A. Al-Saad, "Identification and upgrading of Feldspar in some sand deposits southern Iraq," *Basrah Researches Sciences Journal*, vol. 36, no. 2B, pp. 12–35, 2010.
- [45] Q. Chen, P. Degrange, M. Y. Gerchikov, Z. K. Hillis, S. Lepicard, E. I. M. Meijne, K. R. Smith, and A. Van Weers, "Effluent and Dose Control from European Union NORM Industries-Assessment of Current Situation and Proposal for a Harmonised Community Approach-Volume 1: Main Report," *Radiation Protection*, vol. 135, p. 75, 2003.